Dynamic clustering of passive colloids in dense suspensions of motile bacteria

Shreyas Gokhale, Junang Li, Alexandre Solon, Jeff Gore, and Nikta Fakhri

Phys. Rev. E **105**, 054605 — Published 16 May 2022

DOI: 10.1103/PhysRevE.105.054605

Dynamic clustering of passive colloids in dense suspensions of motile bacteria

Shreyas Gokhale[‡,1] Junang Li[‡,1] Alexandre Solon,[2] Jeff Gore,[1,*] and Nikta Fakhri[1,†]

[1] *Department of Physics, Massachusetts Institute of Technology, Cambridge, MA 02139, USA*

[2] *Sorbonne Université, CNRS, Laboratoire de Physique Théorique de la Matière Condensée, LPTMC, F-75005 Paris, France*

(Dated: April 20, 2022)

Mixtures of active and passive particles are predicted to exhibit a variety of nonequilibrium phases. Here we report a dynamic clustering phase in mixtures of colloids and motile bacteria. We show that colloidal clustering results from a balance between bond breaking due to persistent active motion and bond stabilization due to torques that align active particle velocity tangentially to the passive particle surface. Furthermore, dynamic clustering spans a broad regime between diffusivity-based and motility-induced phase separation that subsumes typical bacterial motility parameters.

I. INTRODUCTION

Collective self-organization of self-propelled, or active, particles is a vibrant topic of research in statistical physics [1, 2]. Active matter exhibits diverse nonequilibrium phenomena including flocks [3], living crystals [4, 5], active nematics [6–9], turbulent phases [10], whorls [11] and nonreciprocal interactions [12]. Recent years have seen a growing interest in interactions between active and passive particles [13], which have been studied in the context of diffusion [14–16], transport [17, 18], pairwise interactions [19, 20] and active dopants [21, 22]. Further, theoretical work on active-passive mixtures predicts segregation based on differences in motility [23–25] or diffusivity [26, 27]. Despite considerable theoretical interest and a growing body of numerical studies, the dynamics and phase behavior of mixtures of active and passive particles remain underexplored experimentally. Furthermore, a majority of studies have focused on the two extreme limits of low and high persistence of active motion. However, synthetic as well as natural active particles such as active colloids and motile bacteria typically exhibit an intermediate level of persistence, and are therefore likely to deviate from the predicted phenomenology in these limits. In a broader context, the mechanisms governing nonequilibrium self-assembly of active-passive mixtures are not yet fully understood. Here, we address these key challenges using experiments on colloids and motile bacteria, as well as Brownian dynamics simulations of active-passive mixtures.

II. EXPERIMENTAL SETUP AND METHODS

Our experiments employ a quasi-2D geometry, with passive silica colloids of diameter $\sigma = 3.2\,\mu$m confined between two coverslips separated by a gap of $5\,\mu$m using spacer particles (Fig. 1a). We held the area fraction of passive colloids constant at $\phi_{\mathrm{p}} = 0.15$, and systematically varied the bacterial density ρ_{b}. We work with low ϕ_{p} to preclude aggregation effects in the absence of bacteria.

A. Bacterial strains and growth conditions

We used motile *Pseudomonas aurantiaca* bacteria as active particles and restricted our experiments to bacterial densities below the onset of active turbulence [10]. *P. aurantiaca* cells are rod shaped, with a long axis of $\approx 1.5\mu$m and aspect ratio ≈ 2. Prior to the experiments, *P. aurantiaca* bacteria (strain ATCC # 33663 with chromosomal insertion miniTn7-GmR-F1-06RFP for expression of red fluorescent protein (RFP)) were streaked from a frozen glycerol stock stored at -80 degree C onto plates containing 2% w/v Luria-Bertani (LB) medium and 1.5% w/v agar (both Beckton, Dickinson and Company, Franklin Lakes, NJ, USA). The plate was incubated for 24 hours at $30°C$. To grow bacteria for microscopy experiments, individual colonies from the plate were used to inoculate 5 mL of growth medium containing 10 g/L Yeast Extract and 10 g/L Soytone (both Beckton, Dickinson and Company, Franklin Lakes, NJ, USA). Prior to inoculation, the growth medium was sterilized by passing through a 0.22 μm filter (VWR), and the pH was adjusted to 7 by dropwise addition of 100 mM sodium hydroxide (NaOH). Bacteria were grown for 16 hours using an orbital shaker at $30°C$ and 250 rpm and allowed to reach saturation density ($\rho_0 = 3 \times 10^9$ colony forming units (CFU) per mL). Throughout the paper, we report the bacterial density ρ_{b} in units of the saturation density ρ_0. The bacterial culture was concentrated by centrifuging at $4000g$ for three minutes. Different bacterial densities were achieved by removing different amounts of supernatant. To test the generality of our findings, we also performed experiments with motile *Escherichia coli* bacteria, using the strain M3K2R: W3110 containing the plasmid pSBIK3-RFP that confers resistance to kanamycin and enables expression of RFP. *E. coli* cells are also rod shaped with aspect ratio ≈ 2, and a long axis of $\approx 2.2\mu$m, and grow to a saturation density $\rho_0 = 7\times10^9$ CFU/mL.

* Corresponding author: gore@mit.edu

† Corresponding author: fakhri@mit.edu

B. Sample and chamber preparation for microscopy experiments

Unfunctionalized silica colloids of diameter $\sigma = 3.2\,\mu$m were purchased either from Bangs Laboratories, Inc. or microParticles GmbH. To demonstrate the interaction between individual Pseudomonas aurantiaca cells and colloids (Video S3), we grew a fluorescent silica shell on the colloids that incorporated the fluorophore rhodamine B isothiocyanate (Sigma Aldrich) using the protocol devised by Kuijk et al. [28]. Video S2 and Video S3 were captured using a customized fluorescence microscope with an EMCCD camera (ANDOR ixon 897) and 100X oil immersion objective lens (Nikon) at 20 frames per second (fps). Unfunctionalized silica colloids of diameter $5\,\mu$m, to be used as spacers, were purchased from Bangs Laboratories, Inc. The $\sigma = 3.2\,\mu$m colloids were concentrated 2X by centrifugation and $5\,\mu$m silica colloids were diluted $10\times$ in distilled deionized water. Prior to the experiments, both types of colloids were sonicated for 30 minutes, in order to break any clusters formed due to sedimentation during storage. 20 μL concentrated bacterial culture, 20 μL of 2X suspension of $3.2\,\mu$m colloids and 1 μL of 0.1X suspension of $5\,\mu$m colloids were mixed together by vortexing at 1500 rpm.

In all experiments, 5 μL of this bacteria-colloid mixture was put between two polymer coverslips (ibidi GmbH, untreated), plasma cleaned at maximum radio frequency (RF) level for 15 minutes before use, filling an area of 18 mm $\times$ 18 mm. The polymer coverslips allow exchange of oxygen with the environment and help maintain bacterial motility over durations several times longer than those of our experiments. The chamber was pressed by placing a known weight of 600g on top of the coverslips for 30 s, which caused the $\sigma = 5\,\mu$m colloids to stick to the top as well as bottom coverslip, thus serving the purpose of spacers. This arrangement ensures that the $\sigma = 3.2\,\mu$m colloids experience quasi-2D confinement. Finally, the chamber was sealed with valap to prevent flows and evaporation. All experiments were performed in triplicate, using different bacterial colonies (biological replicates) and on separate days, to ensure that the observed phenomena are robust to fluctuations in bacterial density, motility and metabolism.

The samples were imaged in bright field with a 40X or 60X air objective on a Motic AE2000 inverted microscope. Videos were acquired for 5 minutes at 6 fps using a CMOS digital camera (AmScope MU500). Prior to capturing videos, we waited for 15 minutes to allow any incidental bulk flows in the sample chamber to subside. The field of view typically contained $\sim 600 \pm 50$ colloids.

III. RESULTS AND DISCUSSION

A. Motile bacteria drive steady state dynamic clustering of passive colloids

While colloids are distributed homogeneously in the absence of bacteria, they undergo significant clustering at high ρ_b (Fig. 1b-c, Video S1). To identify clusters, colloids were localized and tracked using Blair and Dufresne's publicly available Matlab version of the particle tracking code originally developed by Crocker and Grier [29]. Particle trajectories were de-drifted to remove the effects of residual bulk flows in the sample as well as any drift in the microscope stage. Clusters were identified using a distance cutoff. Throughout this study, unless stated otherwise, we classify any two colloids separated by less than 1.2σ, where σ is the colloid diameter, as belonging to the same cluster. Accordingly, the default cutoff distance in our Brownian dynamics simulations is chosen to be $1.2d_\mathrm{p}$, where d_p is the diameter of passive particles. Choosing the cutoff distance to be too small (1.1σ) makes the measurements sensitive to errors in particle localization as well as polydispersity and synthesis defects in the purchased colloids, which increases noise and obscures trends (Fig. S1) [30]. On the other hand, a higher cutoff distance (1.3σ) influences the measured values of mean cluster size and bond lifetimes but leaves our results qualitatively unchanged (Fig. S1) [30]. Thus the phenomenon of dynamic clustering is robust to small changes in the distance cutoff used to define clusters.

We first verified that the clustering is not induced by metabolites produced by the bacteria, by performing a control experiment. For this experiment, after concentrating the bacteria, we filtered the supernatant containing the conditioned growth medium through a 0.2 μm syringe filter (Pall Corporation) to remove bacterial cells. We mixed 20 μL of this filtered supernatant with 20 μL of 2X suspension of 3.2 μm colloids and 1 μL of 0.1X suspension of $\sigma = 5\,\mu$m colloids and loaded 5 μL of this sample into the same type of imaging chamber as described above. These conditions are identical to those in our main experiments, with the exception that the bacterial suspension is replaced by the conditioned growth medium. We then took a time lapse video at 1 frame per minute for 250 minutes, which is 50 times longer than the duration of our experiments. We observed no evidence of colloidal clustering over this period (Fig. S2) [30], showing that the clustering observed in our experiments is due to bacterial motility alone, and not due to chemical modifications in the growth medium that occur during bacterial growth.

Clustering results in strong enhancement of the first peak of the radial distribution function $g(r)$ (Fig. 1d). Furthermore, the cluster size distribution $P(n)$, n being the number of colloids in a cluster, becomes significantly broader for high ρ_b (Fig. 1e), resulting in a larger mean cluster size $\langle n \rangle = \sum nP(n)$ (Fig. 1e, inset). We quantified the broadening of $P(n)$ by computing the probability

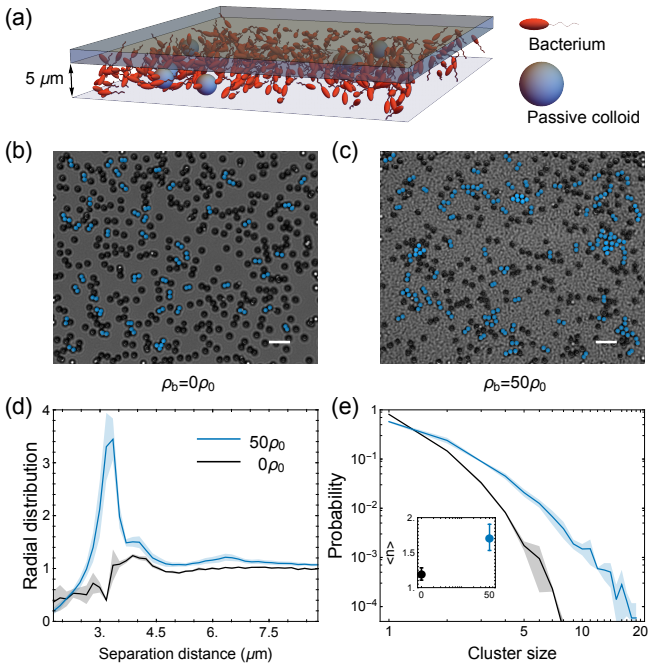

FIG. 1. **Dynamic clustering of passive colloids by motile bacteria.** (a) Schematic of the experimental setup. (b-c) Representative snapshots of colloids at $\rho_b = 0$ (b) and $\rho_b = 50\rho_0$ (c). Monomers are shown in black, and clusters in blue, with lighter shades indicating larger clusters. The scale bar is 10μm. (d) $g(r)$ for $\rho_b = 0$ (black) and $\rho_b = 50\rho_0$ (blue). (e) $P(n)$ for $\rho_b = 0$ (black) and $\rho_b = 50\rho_0$ (blue). Inset shows the mean cluster size computed from data in the main plot. Shaded regions in (d) and (e) and error bars in inset to (e) are standard errors of the mean across three independent experiments.

of clustering, $P(n > 2)$, defined as the fraction of clusters containing at least three colloids (Fig. S3) [30]. Consistent with increasing $\langle n \rangle$, we observe that $P(n > 2)$ at $\rho_b = 50\rho_0$ is four times as large as that for $\rho_b = 0$. Furthermore, we observe qualitatively similar clustering with *Escherichia coli* bacteria as well, demonstrating that the phenomenon is general and robust (Fig. S4) [30].

While clusters form and break over seconds, $\langle n \rangle$ does not evolve over 30 minutes, suggesting that the system is in a nonequilibrium quasi-steady state (Fig. S5) [30]. This dynamic steady state is characterized by a monotonically decaying $P(n)$ (Fig. 1e and Fig. S6) [30], which is substantially different from the phase separation of active and passive particles predicted in previous studies. A key parameter that determines phase behavior of active particles is the Péclet number $Pe = v_a \tau_r / d_a$ where v_a is the speed of active particles, τ_r is a reorientation time scale set by rotational diffusion for active Brownian particles or tumbling time for bacteria, and d_a is the size of the active particles. At high Péclet numbers ($Pe \gg 1$), mixtures of active and passive particles are expected to undergo segregation [23–25] accompanied by large inhomogeneities in active particle density, consistent with motility-induced phase separation (MIPS) in purely active systems [31]. However, numerical studies have shown that MIPS is not observed in 2D below $Pe \approx 55$ [31]. Since the measured Péclet number for our bacteria is much smaller ($Pe \approx 14$, Fig. S7), we do not expect MIPS-like segregation to occur in our system [30]. Furthermore, the presence of passive particles increases the critical Péclet number for MIPS [24]. We therefore do not observe any spatial inhomogeneity in bacterial density even at $\rho_b = 50\rho_0$, the highest density studied (Video S2). Phase separation can also occur in mixtures of particles that differ significantly in their diffusivities [26, 27]. For active-passive mixtures, this occurs for $Pe < 1$. However, the Péclet number for our bacteria is large enough to suppress diffusivity-based phase separation completely. The observed steady state dynamic clustering is a distinct effect that has neither been predicted nor observed before.

B. Brownian dynamics simulations of active and passive disks with aligning torques recapitulate dynamic clustering

To understand the origin of dynamic clustering, we investigated a minimal model system consisting of active and passive Brownian disks of diameter d_a and d_p respectively, in two dimensions (Fig. 2a). Both types of particles obey an overdamped Langevin equation in two spatial dimensions. The position $\mathbf{r}_i$ of passive particle i follows

$$\frac{d\mathbf{r}_i}{dt} = \mu_p \mathbf{F}_i + \sqrt{2D_{t,p}}\boldsymbol{\xi}_i \tag{1}$$

where μ_p is the mobility of a passive particle, $\boldsymbol{\xi}_i$ a 2D Gaussian white noise with unit variance and $D_{t,p}$ the coefficient of translational diffusion of a passive particle. In addition, the active particles self-propel at a speed v_0, thus following

$$\frac{d\mathbf{r}_i}{dt} = v_0 \mathbf{u}_i + \mu_a \mathbf{F}_i + \sqrt{2D_{t,a}}\boldsymbol{\xi}_i \tag{2}$$

where μ_a and $D_{t,a}$ are the mobility and translational diffusion coefficient of an active particle, respectively. $\mathbf{u}_i = (\cos\theta_i, \sin\theta_i)$ is a unit vector giving the direction of propulsion of particle i. It is parametrized by an angle θ_i subject to rotational diffusion with coefficient D_r and to torques that tend to align tangentially to the surface of the passive particles

$$\frac{d\theta_i}{dt} = -\Gamma \sum_j \sin(\theta_i - \theta_{ij}) + \sqrt{2D_r}\eta_i \tag{3}$$

where the sum runs over passive particles in contact with particle i (main text Fig. 2a). Γ sets the speed of alignment, $\theta_{ij} = \arg(\mathbf{r}_i - \mathbf{r}_j)$ and η_i is a Gaussian white noise of unit variance. This type of interaction is standard to model the alignment of self-propelled rods with the surface of passive objects [32]. Our minimal model

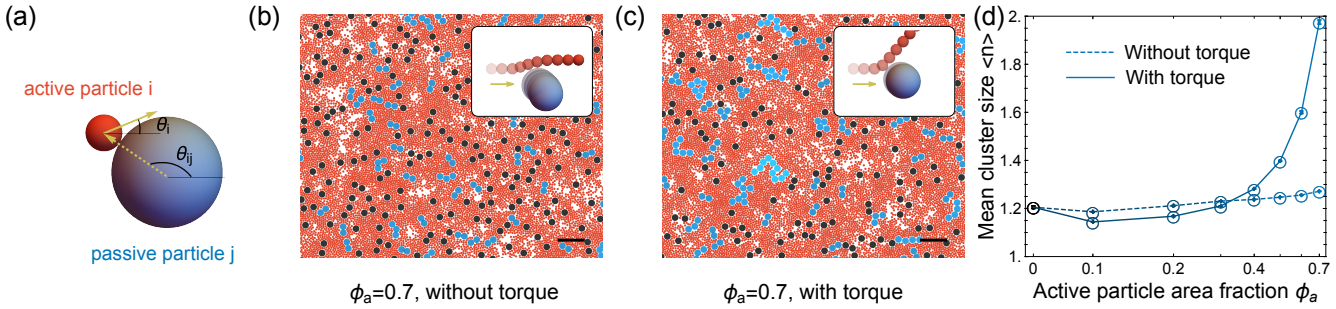

FIG. 2. **Torque-induced stabilization of clusters in simulations.** (a) Schematic showing the orientation of active particles parametrized by θ_i, and θ_{ij} is the orientation of the relative position vector between active particle i and passive particle j. (b-c) No clustering is observed for $\Gamma = 0/\mathrm{s}$ (b) but substantial clustering is observed at $\Gamma = 25/\mathrm{s}$ (c). Monomers are shown in black, and clusters in blue, with lighter shades indicating larger clusters. Insets in (b) and (c) reveal the difference in particle trajectories during a collision, with (c) and without (b) torque. The scale bar is 10μm.(d) Mean cluster size as a function of ϕ_a for $\Gamma = 0/\mathrm{s}$ (dotted line) and $\Gamma = 25/\mathrm{s}$ (solid line). In (b-d), error bars are standard errors of the mean across three independent simulations.

replaces short-ranged hydrodynamic lubrication interactions by contact interactions. This simplification is justified, since previous work has shown that the measured value of Γ for swimming bacteria matches the estimated value from contact interactions within experimental error [33]. Finally, the interaction F_i in Eqs. (1)-(2) accounts for volume exclusion. It derives from a potential so that $\mathbf{F}_i = -\nabla_{r_i} U$ with

$$U = -\frac{k}{2}\sum_{i<j}\left(\frac{d_i+d_j}{2} - |\mathbf{r}_i - \mathbf{r}_j|\right)^2 \Theta\left(\frac{d_i+d_j}{2} - |\mathbf{r}_i - \mathbf{r}_j|\right) \tag{4}$$

where d_i and d_j assume the value d_a for active particles and d_p for passive ones. The Heaviside Θ function insures that particles interact only when they are in contact, *i.e.* when the distance between them is less than the sum of their radii. Eq. (4) imposes a soft harmonic repulsion between the particles but in practice we take a large $k = 100$ that allows for little overlap. Throughout the paper, we choose $d_\mathrm{a} = 1\mu$m, $d_\mathrm{p} = 3\mu$m, $v_0 = 10\mu\mathrm{m/s}$, $\mu_\mathrm{a} = (d_\mathrm{p}/d_\mathrm{a})\mu_\mathrm{p} = 1\mathrm{mPa}^{-1}\cdot\mathrm{s}^{-1}\cdot\mu\mathrm{m}^{-1}$,and $D_{\mathrm{t,a}} = (d_\mathrm{p}/d_\mathrm{a})D_{\mathrm{t,p}} = 0.15\mu\mathrm{m}^2/\mathrm{s}$.

Simulations of our model system with $\Gamma = 0/\mathrm{s}$ show that motility alone is not sufficient to induce significant clustering, even for very high area fractions of active particles ϕ_a (Fig. 2b). However, we observe the formation of clusters for $\Gamma = 25/\mathrm{s}$ (Fig. 2c). Moreover, as in the experiments, the clustered phase is a nonequilibrium steady state (Fig. S8) with a monotonically decaying $P(n)$ (Fig. S9) [30]. Interestingly, dynamic clustering is qualitatively robust to changes in the relative size of active and passive particles. Simulations with $d_\mathrm{p} = 0.5d_\mathrm{a}$ exhibit clustering with significantly larger $\langle n\rangle$ (Fig. S10) [30]. Elucidating the effect of particle size ratio on clustering is an interesting topic for future research. The inclusion of Γ in our simulations is motivated by anisotropic bacterial shape and flow fields [34], which lead them to turn away from colloids on contact [33] (Video S3) [30]. Furthermore, we observe that $\langle n\rangle = \sum nP(n)$ increases substantially with ϕ_a in the presence of torque ($\Gamma = 25/\mathrm{s}$), but remains nearly constant for $\Gamma = 0/\mathrm{s}$ (Fig. 2d).

Fig. 2 shows that although torque only acts on active particles, it strongly influences dynamic clustering. This is because the magnitude of torque controls the momentum transferred to passive particles during collisions with active ones (insets to Fig. 2b-c. Also see Video S4) [30]. Finite Γ leads to faster reorientation of active particles (Fig. 2c, inset), and consequently a smaller "push" on passive particles compared to $\Gamma = 0/\mathrm{s}$ (Fig. 2b, inset). We quantified this effect by measuring the effective single-particle diffusivity of passive particles as a function of Γ, for a fixed $\phi_\mathrm{a} = 0.6$ (Fig. S11) [30]. As expected, effective diffusivity decreases strongly with Γ. Crucially, the torque-induced reduction of momentum transfer plays a significant role in stabilizing larger clusters. To illustrate this fact, we initialized our simulations with a single large cluster of passive particles in the center of the simulation box, surrounded by a sea of active particles. For $\Gamma = 0/\mathrm{s}$, the cluster dissolves rapidly, whereas with increasing torque, it dissolves over increasingly longer timescales (Video S5) [30].

C. Dynamic clustering results from torque-induced effective attractions between passive particles

To gain further insights into the mechanism of clustering, we numerically investigated the diffusion and bonding kinetics of passive particles for various ϕ_a. To avoid possible many body effects, we extract the diffusion coefficient of passive particles by simulating a single passive particle in a bath of active particles, and averaging over time. Likewise, to quantify bond lifetimes, we simulated two passive particles diffusing in a bath of active particles and generated a bond lifetime distribution from

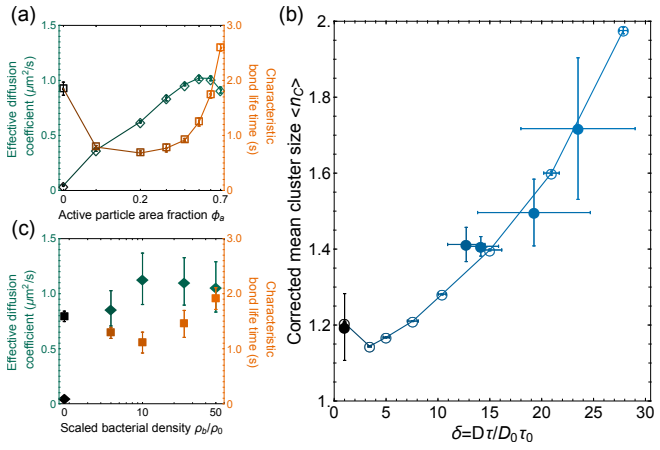

FIG. 3. **Effective attraction between passive particles leads to clustering.** (a) Effective diffusivity (open green diamonds) and bond lifetime (open orange squares) of passive particles versus ϕ_a in simulations. (b) Mean cluster size versus $\delta = D\tau/(D_0\tau_0)$ in simulations (open symbols) and experiments (filled symbols). (c) Effective diffusivity (filled green diamonds) and bond lifetime (filled orange squares) of colloids versus ρ_b/ρ_0 in experiments. In (a-c), black symbols correspond to $\phi_a = 0$ in simulations and $\rho_b = 0$ in experiments. Error bars in (a-c) are standard errors of the mean from three independent replicates.

several independent bonding events, assuming that the two particles are bonded, if the separation between them is less than $1.2d$. Collisions with active particles enhance diffusion of passive ones, which opposes clustering. However, for $\Gamma > 0/\mathrm{s}$, the same collisions also result in effective attractions between pairs of passive particles, leading to cluster formation. We quantified these competing effects using the single particle diffusivity D (Fig. 3a, open green diamonds) and the mean pair bond lifetime τ (Fig. 3a, open orange squares) for passive particles (Also see Fig. S12-S13) [30]. Using the corresponding quantities D_0 and τ_0 under thermal fluctuations for $\phi_a = 0$, we constructed a dimensionless parameter $\delta = D\tau/(D_0\tau_0)$ that serves as an indicator of the strength of effective attractions. In the absence of attractions, enhancement in diffusion would be accompanied by a corresponding decrease in bond lifetimes, resulting in $\delta \sim 1$. However, attractive interactions can lead to a substantial increase in lifetimes, leading to $\delta \gg 1$. We therefore expect that larger δ should result in larger clusters, which is indeed observed in our simulations (Fig. 3b, open symbols).

Finally, we examined whether the predicted increase in $\langle n \rangle$ with δ can also be observed in experiments. To extract the effective diffusion coefficient of colloids in our experiments, we calculated the mean square displacement using a time average for a single track as well as an ensemble average over the tracks of all colloids in the field of view. While the diffusion coefficient is a property of individual colloids, its measurement can be affected by the clustering observed in our experiments. To remove the effect of clustering on diffusivity measurements, we only considered those particle trajectories that had on average less than one nearest neighbor over their duration. Nearest neighbors were defined using the same distance cutoff used to identify clusters. The MSDs for all bacterial densities studied were diffusive at long times (Fig. S14) [30], which allowed us to extract the diffusion coefficient of colloids.

To quantify bond lifetimes in experiments, we assume that two colloids are bonded to each other if their centroids are separated by a distance smaller than 1.2σ, the same cutoff distance used for clustering analysis. A bond lifetime for a pair of colloids is defined as the duration over which two colloids remain separated by a distance smaller than 1.2σ. The bond is said to be broken once the separation exceeds this cutoff distance. Two colloids can thus form and break bonds with each other as well as with other colloids, several times during the experiment. While bond lifetimes can help us quantify effective pairwise interactions, these can also be affected by clustering, since particles in the interior of clusters will typically have longer bond lifetimes. Thus, clustering leads to heavy tails in the bond lifetime distributions (Fig. S15) [30]. We ignore these heavy tails and only consider the initial exponential decay of bond lifetimes in order to get a more accurate estimate of the characteristic bond lifetime of pairs of colloids. The characteristic bond lifetime is defined as the decay constant of the exponential fit to the initial decay of the bond lifetime distribution.

We observe that the variation in D (Fig. 3c, filled green symbols) and τ (Fig. 3c, filled orange symbols) with ρ_b is qualitatively similar to that observed in simulations (Fig. 3a), particularly from moderate to high ϕ_a. Next we quantified the mean cluster size from our experimental data. While $\phi_p \approx 0.15$ in our experiments, in practice, the number of colloids in the field of view fluctuates across replicates, which influences our measurements of the mean cluster size. To account for these fluctuations, we define a corrected mean cluster size $\langle n_C^i \rangle = \frac{\langle N \rangle}{N_i}\langle n \rangle$, where $\langle n \rangle$ is the measured mean cluster size, $\langle N \rangle$ is the number of colloids in the field of view averaged across all experimental replicates and all bacterial densities, and N_i is the number of colloids in the field of view for the i^{th} experiment, averaged over the experimental duration. Both the bare as well as corrected mean cluster size increase with ρ_b (Fig. S16) [30]. Experiments with *E. coli* also show qualitatively similar results (Fig. S4) [30]. $\langle n_C^i \rangle$ plotted as a function of δ (Fig. 3b, filled symbols), is in agreement with the prediction from simulations, demonstrating that the clustering mechanism revealed by our simulations can adequately explain our experimental findings.

D. Dynamic clustering spans a wide range of parameters in the Alignment rate - Péclet number plane

To better understand the effect of torques, and place our results in the context of prior work on mixtures of active and passive particles [23–27], we construct a numerical phase diagram for our system in the Pe-Γ plane, keeping $\phi_{\rm p} = 0.15$ and $\phi_{\rm a} = 0.6$ fixed. We delineate different phases using two order parameters. First we define an order parameter for the demixed regime $O_{\rm DM} = \langle N_L/N_p \rangle_t$, where N_L is the number of particles in the largest cluster of passive particles, N_p is the total number of passive particles, and $\langle\rangle_t$ indicates time averaging. We also define a MIPS order parameter $O_{\rm MIPS} = \langle \sigma_\phi \rangle_t/(\phi_{\rm a} + \phi_{\rm p})$, where σ_ϕ is the standard deviation of the local area fraction ϕ, computed by dividing the simulation box into square cells of length $5d_{\rm a}$. As expected [26, 27], we observe a demixed phase at low Pe (Fig. 4a-b), clustered phase at intermediate Pe (Fig. 4a,c) and motility-induced phase separation [31] at high Pe (Fig. 4a,d) (See Fig. S17 for representative snapshots of simulated data points and Video S6 for movies corresponding to Fig. 4b-d [30]). Qualitatively, increasing Γ shifts the demixed as well as MIPS phase boundaries to higher Pe (Fig. 4a), suggesting that aligning torques effectively reduce the persistence of active motion. The effect of torque-induced interactions on MIPS in purely active systems has been studied in previous numerical works [35–37]. Specifically, it has been shown that while torques that lead to velocity alignment promote MIPS [36, 37], torques resulting from elongated shapes of active particles suppress MIPS by reducing the duration of collisions [35]. Our findings are consistent with those of [35], with the important distinction that in our experiments, suppression of MIPS happens due to torques associated with collisions between active and passive particles, rather than between two active particles.

Over a wide range of Pe and Γ, we generically observe the dynamic clustering phase, with a mean cluster size that increases with Γ (Fig. S18) [30]. Using experimental measurements of speed ($v_b \approx 40\mu$m/s), cell size ($d_b \approx 1.5\mu$m), and tumbling time (≈ 0.5s), we estimate $Pe \approx 14$ and $\Gamma \sim v_b/d_b \approx 27$/s for *P. aurantiaca* bacteria (Fig. S7) [30]. For *E. coli*, our measurements yield swim speed $v_b \approx 16\mu$m/s, cell size $d_b \approx 2.2\mu$m, and tumbling time (≈ 0.5s), resulting in $Pe \approx 4$ and $\Gamma \sim v_b/d_b \approx 7$/s (Fig. S7) [30]. The motility parameters for both species of bacteria thus lie within the numerically predicted dynamic clustering regime (Fig. 4a, stars). Indeed, since most motile bacteria exhibit sizes $\sim 1\mu$m, speeds $\sim 10\mu$m/s and tumbling times ~ 1s, we expect dynamic clustering to be a generic feature of bacterial active matter.

To conclusively demonstrate that dynamic clustering of passive colloids is an independent phenomenon distinct from MIPS, we performed fluorescence video microscopy on our *P. aurantiaca* bacteria. Visually, we observe that

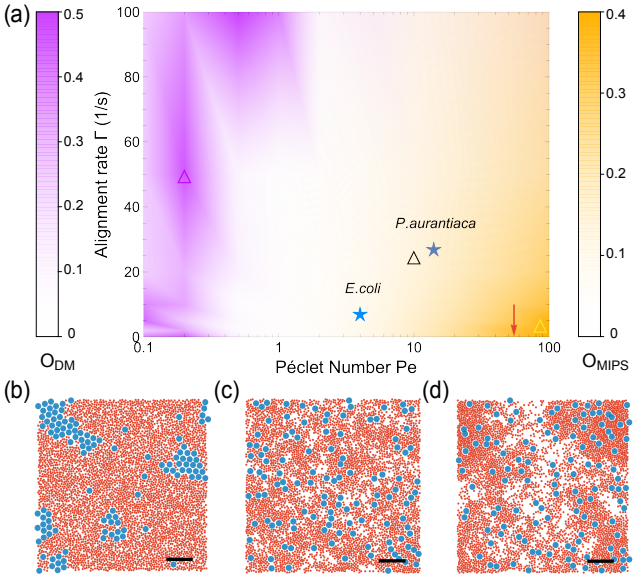

FIG. 4. **Numerical phase diagram of mixtures of active and passive particles** (a) Phase diagram in the Péclet number (Pe) - alignment rate (Γ) plane showing diffusivity-based phase separation at low Pe (purple region), dynamic clustering at intermediate Pe (white region), and MIPS at high Pe (yellow region). The purple colormap (left) corresponds to the demixed phase order parameter ($O_{\rm DM}$), and yellow colormap (right) corresponds to the MIPS order parameter ($O_{\rm MIPS}$). The stripes in the purple region result from sparse sampling of the parameter space and incomplete domain coarsening due to the finite duration of simulations. The red arrow corresponds to $Pe = 55$, the critical Péclet number for the onset of MIPS in 2D [31]. Blue stars correspond to experimental data points for *P. aurantiaca* and *E. coli* bacteria. (b-d) Representative simulation snapshots of the demixed phase (b), clustered phase (c), and MIPS phase (d). Triangles in (a) denote the values of Pe and Γ used for the simulations in (b-d). The scale bar is 10μm.

bacteria are uniformly distributed throughout the field of view and do not exhibit the pronounced density fluctuations expected for MIPS (Video S2) [30]. The absence of MIPS could stem from a number of factors such as the low Péclet number, hydrodynamic effects [31],torque-induced effects [35], as well as the presence of passive colloids [24]. To quantify bacterial density fluctuations, we define a modified version of the MIPS order parameter described earlier, $O^I_{\rm MIPS}$, defined as $O^I_{\rm MIPS} = \langle \sigma_I/I_{avg} \rangle_t$, where σ_I is the standard deviation of the local fluorescence intensity I, computed by dividing the field of view into square cells of length $5d_b$, and I_{avg} is the fluorescence intensity averaged over the full image. To avoid artifacts due to non-uniform sample illumination, we restricted our analysis to a 240 pixel × 240 pixel (38.4μm × 38.4μm) square region including the bottom right corner of the field of view. Our analysis yields a very low value of $O^I_{\rm MIPS} = 0.07 \pm 0.015$, demonstrating that the active phase of our system is not in the MIPS regime. Further-

more, a bright field video of the same field of view taken immediately after the fluorescence video shows clusters of silica colloids, showing that the system is in fact in the dynamic clustering regime (Video S2) [30].

IV. CONCLUSION AND OUTLOOK

In summary, we have shown that passive colloids exhibit steady state dynamic clustering when immersed in a bath of motile bacteria, and that clustering can be tuned by changing the bacterial density (Fig. 1). Using Brownian dynamics simulations of active and passive disks, we have shown that torques experienced by active particles on collisions with passive ones are sufficient to stabilize the observed micro phase separated state. The quantitative agreement between experiments and simulations (Fig. 3b) further strengthens this claim. Crucially, dynamic clustering represents a distinct nonequilibrium phase in the phenomenology of active-passive mixtures that spans a broad range of Péclet numbers (Fig. 4a) between the two well-studied limits associated with diffusivity based demixing and motility induced phase separation. Our work provides the first experimental observation as well as numerical characterization of this phase. Our study further reveals that in addition to the Péclet number, torque, as quantified by the the alignment rate Γ, serves as an important parameter for characterizing active systems.

The physical picture underlying dynamic clustering can be understood by approaching from the low Péclet number regime, where demixing is driven by diffusivity differences [26, 27]. In this regime, particles with high diffusivity are unable to break clusters of particles with low diffusivity due to rapid stochastic reorientation of their velocity vectors, which results in complete phase separation. Persistent active motion at intermediate Péclet numbers is sufficient to break these clusters rapidly enough for the system to be completely disordered (Fig. 2b). The addition of torque leads to a faster reorientation of the active particles, which reduces the propensity of active motion to break clusters, thereby resulting in micro phase separation, or steady state dynamic clustering (Fig. 2c). While bonds between passive particles can always be formed in mixtures of active and passive particles due to collisions, whether the system undergoes complete phase separation, micro phase separation, or remains completely disordered, depends on the timescales over which those bonds persist. Dynamic clustering therefore results from a balance between persistent active motion, which leads to breaking of clusters, and torque, which leads to stabilization of clusters (Video S5).

At the two body level, the stabilizing effect of torques can be interpreted as an effective attraction between passive particles, as evidenced by the enhancement of bonding times relative to the expectation based on diffusion alone (Fig. 3b). However, in the presence of pairwise attractions alone, the system would undergo complete phase separation, instead of micro phase separation. This suggests that many body interactions that destabilize large clusters must also be present. It would be interesting to investigate the nature of these effective many body interactions in future works. Nonetheless, the presence of effective attractions suggests a possible route to direct and manipulate the self-assembly of building blocks by simultaneously tuning inter-particle interactions as well as spatiotemporal correlations in the active bath. Furthermore, using passive particles that break fore-aft [38] or chiral [39] symmetry, it should be possible to self-assemble ordered structures with intrinsic translational or rotational dynamics, which cannot exist in equilibrium.

ACKNOWLEDGMENTS

S.G. was supported by a Human Frontier Science Program (HFSP) cross-disciplinary postdoctoral fellowship though Grant No. LT000470/2016-C. S.G. and A.S. acknowledge the Gordon and Betty Moore Foundation for support as Physics of Living Systems Fellows through Grant No. GBMF4513. This research was supported by the Sloan Foundation Grant (G-2021-16758) to N.F. and J.G., and in part by the National Science Foundation under Grant No. NSF PHY-1748958 (to N.F.) .

[‡]S.G and J.L contributed equally to this work.

[1] M. C. Marchetti, J.-F. Joanny, S. Ramaswamy, T. B. Liverpool, J. Prost, M. Rao, and R. A. Simha, Reviews of Modern Physics **85**, 1143 (2013).
[2] M. J. Bowick, N. Fakhri, M. C. Marchetti, and S. Ramaswamy, arXiv preprint arXiv:2107.00724 (2021).
[3] A. Bricard, J.-B. Caussin, N. Desreumaux, O. Dauchot, and D. Bartolo, Nature **503**, 95 (2013).
[4] J. Palacci, S. Sacanna, A. P. Steinberg, D. J. Pine, and P. M. Chaikin, Science **339**, 936 (2013).
[5] T. H. Tan, A. Mietke, H. Higinbotham, J. Li, Y. Chen, P. J. Foster, S. Gokhale, J. Dunkel, and N. Fakhri, arXiv preprint arXiv:2105.07507 (2021).
[6] V. Narayan, S. Ramaswamy, and N. Menon, Science **317**, 105 (2007).
[7] T. Sanchez, D. T. Chen, S. J. DeCamp, M. Heymann, and Z. Dogic, Nature **491**, 431 (2012).
[8] G. Duclos, R. Adkins, D. Banerjee, M. S. Peterson, M. Varghese, I. Kolvin, A. Baskaran, R. A. Pelcovits, T. R. Powers, A. Baskaran, et al., Science **367**, 1120 (2020).
[9] K. Copenhagen, R. Alert, N. S. Wingreen, and J. W. Shaevitz, Nature Physics **17**, 211 (2021).

[10] H. H. Wensink, J. Dunkel, S. Heidenreich, K. Drescher, R. E. Goldstein, H. Löwen, and J. M. Yeomans, Proceedings of the national academy of sciences **109**, 14308 (2012).

[11] E. S. Bililign, F. Balboa Usabiaga, Y. A. Ganan, A. Poncet, V. Soni, S. Magkiriadou, M. J. Shelley, D. Bartolo, and W. Irvine, Nature Physics , 1 (2021).

[12] J. Zhang, R. Alert, J. Yan, N. S. Wingreen, and S. Granick, Nature Physics , 1 (2021).

[13] C. Bechinger, R. Di Leonardo, H. Löwen, C. Reichhardt, G. Volpe, and G. Volpe, Reviews of Modern Physics **88**, 045006 (2016).

[14] X.-L. Wu and A. Libchaber, Physical review letters **84**, 3017 (2000).

[15] A. E. Patteson, A. Gopinath, P. K. Purohit, and P. E. Arratia, Soft matter **12**, 2365 (2016).

[16] Y. Peng, L. Lai, Y.-S. Tai, K. Zhang, X. Xu, and X. Cheng, Physical review letters **116**, 068303 (2016).

[17] N. Koumakis, A. Lepore, C. Maggi, and R. Di Leonardo, Nature communications **4**, 1 (2013).

[18] L. Vaccari, M. Molaei, R. L. Leheny, and K. J. Stebe, Soft Matter **14**, 5643 (2018).

[19] L. Angelani, C. Maggi, M. L. Bernardini, A. Rizzo, and R. Di Leonardo, Physical review letters **107**, 138302 (2011).

[20] P. Liu, S. Ye, F. Ye, K. Chen, and M. Yang, Physical review letters **124**, 158001 (2020).

[21] F. Kümmel, P. Shabestari, C. Lozano, G. Volpe, and C. Bechinger, Soft matter **11**, 6187 (2015).

[22] S. Ramananarivo, E. Ducrot, and J. Palacci, Nature communications **10**, 1 (2019).

[23] S. R. McCandlish, A. Baskaran, and M. F. Hagan, Soft Matter **8**, 2527 (2012).

[24] J. Stenhammar, R. Wittkowski, D. Marenduzzo, and M. E. Cates, Physical review letters **114**, 018301 (2015).

[25] P. Dolai, A. Simha, and S. Mishra, Soft Matter **14**, 6137 (2018).

[26] A. Y. Grosberg and J.-F. Joanny, Physical Review E **92**, 032118 (2015).

[27] S. N. Weber, C. A. Weber, and E. Frey, Physical review letters **116**, 058301 (2016).

[28] A. Kuijk, A. Van Blaaderen, and A. Imhof, Journal of the American Chemical Society **133**, 2346 (2011).

[29] J. C. Crocker and D. G. Grier, Journal of colloid and interface science **179**, 298 (1996).

[30] See Supplemental Material at [URL will be inserted by publisher] for supporting data plots..

[31] M. E. Cates and J. Tailleur, Annu. Rev. Condens. Matter Phys. **6**, 219 (2015).

[32] O. Chepizhko, E. G. Altmann, and F. Peruani, Physical review letters **110**, 238101 (2013).

[33] A. Lagarde, N. Dagès, T. Nemoto, V. Démery, D. Bartolo, and T. Gibaud, Soft Matter **16**, 7503 (2020).

[34] D. Giacché, T. Ishikawa, and T. Yamaguchi, Physical Review E **82**, 056309 (2010).

[35] R. Van Damme, J. Rodenburg, R. Van Roij, and M. Dijkstra, The Journal of chemical physics **150**, 164501 (2019).

[36] J. Barré, R. Chétrite, M. Muratori, and F. Peruani, Journal of Statistical Physics **158**, 589 (2015).

[37] E. Sese-Sansa, I. Pagonabarraga, and D. Levis, EPL (Europhysics Letters) **124**, 30004 (2018).

[38] Y. Baek, A. P. Solon, X. Xu, N. Nikola, and Y. Kafri, Physical review letters **120**, 058002 (2018).

[39] A. Sokolov, M. M. Apodaca, B. A. Grzybowski, and I. S. Aranson, Proceedings of the National Academy of Sciences **107**, 969 (2010).